Contract No.:

This manuscript has been authored by Battelle Savannah River Alliance (BSRA), LLC under Contract No. 89303321CEM000080 with the U.S. Department of Energy (DOE) Office of Environmental Management (EM).

ARTICLE

Investigating the Hydrolysis of Cryogenically Layered Molybdenum Hexafluoride Through a Disordered Hydrogen-Bonded Network

Received 00th January 20xx,
Accepted 00th January 20xx

DOI: 10.1039/x0xx00000x

Louis McNamara,[a] Abigail Waldron,[a] Michael Thomas,[a] Willis Jones,[ab] Patrick O'Rourke,[a] Darrell Simmons,[c] and K. Alicia Strange Fessler*[a]

Molybdenum hexafluoride (MoF_6) is used as a non-radioactive substitute for uranium to study the hydrolysis of metal hexafluorides. Molybdenum hexafluoride gas and water vapor, from the air, were sequentially layered onto a diamond substrate kept at liquid nitrogen temperature using a custom designed cryogenic cell with a copper cold finger. Reaction progress was monitored by transmission Fourier Transform Infrared Spectroscopy (FTIR) through the layers and diamond substrate over several hours while allowing the substrate to warm. Changes in the modes in the 500-1000 cm^{-1} region are tracked as the reaction progresses in order to identify intermediate species. Strong absorption features are also observed in the 1000–3000 cm^{-1} range, suggesting the presence of ionic dissociation intermediates trapped in a disordered H-bonded network of cryogenic hydrofluoric acid. A possible reaction pathway is proposed and the final hydrolysis product is characterized by FTIR, UV-Vis, and Scanning Electron Microscopy/Energy Dispersive X-Ray Spectroscopy (SEM/EDS).

Introduction

Uranium hexafluoride (UF_6) is a highly utilized material feedstock for uranium enrichment processes, including gas diffusion, gas centrifuge, and some laser separations. These enrichment processes take advantage of the solid material state of UF_6 at room temperatures and ambient pressures, as well as the ease of sublimation upon heating. As a result of the common use of UF_6 in uranium enrichment since the 1940s, the chemical processing of UF_6 has been highly studied and is well understood[1-8]. However, uranium enrichment is carried-out under controlled conditions to limit moisture in the process to prevent loss of uranium to more thermodynamically favorable reactions which produce solids (material holdup). When UF_6 is exposed to atmosphere, it readily undergoes the hydrolysis reaction $UF_6(g) + 2H_2O(g) \rightarrow UO_2F_2(s) + 4HF(g)$. The reaction pathway of the UF_6 hydrolysis reaction is not well understood, and computationally predicted key intermediates have never been observed experimentally.

Previous research performed at Oak Ridge National Laboratory on uranyl fluoride (UO_2F_2) particulate formation suggests the final product of the reaction is a function of the relative humidity, where small fractal aggregates form when a limited amount of water is available and larger spheroidal particles form at high relative humidity[9, 10]. Historically, research has focused on gas phase spectroscopy to better understand the chemical products of the reaction[11-13], although several studies have characterized the chemical morphology and speciation of the products[14-17]. More significant effort has been applied to computational studies which have aimed to elucidate the reaction dynamics of the hydrolysis reaction[18-24]. Computational studies have primarily predicted the hydrolysis reaction progression through experimentally unobserved intermediates, most commonly UF_5OH.

There is a very limited amount of research on whether the hydrolysis reaction is required to occur: (1) in the gas-phase, creating UO_2F_2 molecules which then cluster to form larger particulates, (2)if initial formation of molecular UO_2F_2 can seed the formation of clusters at earlier times and the reaction then proceeds freely in the condensed phase, or (3) if both pathways are possible. With limited experimental data on the hydrolysis reaction in the condensed phase and no thermodynamic data for UF_5OH, computational studies are unable to definitively assess the role of condensed phase chemistry[24].

In the work described here, the hydrolysis of molybdenum hexafluoride (MoF_6) was studied as a surrogate reaction for the hydrolysis of UF_6 to reduce safety concerns regarding the handling of radioactive material. MoF_6 also readily undergoes hydrolysis when in contact with atmospheric humidity and is a known contaminate in nuclear fuel cycle byproducts. The hydrolysis reaction was studied in the condensed phase under cryogenic conditions to slow down the reaction kinetics and capture possible reaction intermediates. Since particulate formation has only been studies in the gas phase, working in the condensed phase will also elucidate what role condensed phase reactions may have on product particulate formation. A novel

[a] Savannah River National Laboratory, 301 Gateway Drive, Aiken, 29803, SC, United States.
[b] University of North Florida, 1 UNF Drive, Jacksonville, FL 32224, United States.
[c] Oak Ridge National Laboratory, 1 Bethel Valley Road, Oak Ridge, 37830, TN, United States.
Electronic Supplementary Information (ESI) available: [details of any supplementary information available should be included here]. See DOI: 10.1039/x0xx00000x

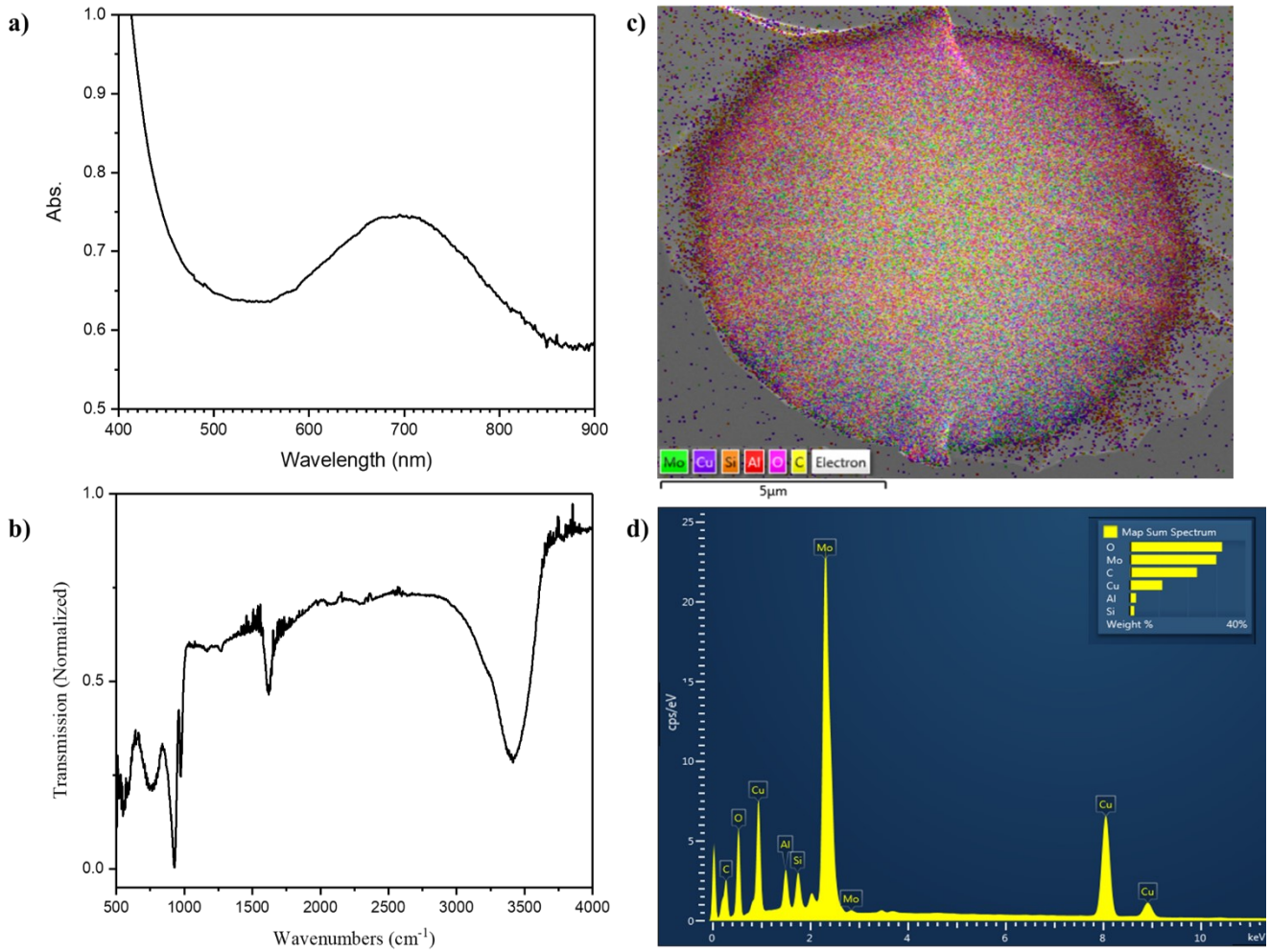

Figure 1 a) UV/visible absorption spectrum of final product dissolved in DI water, b) Transmission FTIR spectrum of product on diamond substrate, c) EDS layered image of product, d) EDS graph of product (Cu, C, Si, and Al are all artefacts from the stage and stage holder).

cryogenic layering technique was used to freeze the reactants to prevent spontaneous hydrolysis and control the rate of the reaction.

The hydrolysis of MoF_6 has received little attention in the literature and this work intends to: (1) demonstrate the ability of our layering technique to track and isolate reaction intermediates, (2) elucidate the reaction pathway governing the hydrolysis of MoF_6, and (3) use the information learned about the hydrolysis of MoF_6 to better understand possible reaction pathways of UF_6 hydrolysis.

Results and Discussion

MoF_6 Hydrolysis Product Characterization

The final product of the hydrolysis of MoF_6 in the condensed phase cryogenic layering experiment was a deep blue film covering the diamond substrate. If MoF_6 hydrolysis were a perfect substitute for UF_6, the expected final product would be MoO_2F_2. However, the product was identified as a hydrate of MoO_3 based on the characteristics of previously reported molybdenum oxide samples in the literature[25-33]. In addition to FTIR, the product was also characterized using UV-Vis and SEM/EDS (Figure 1).

MoF_6 Hydrolysis by Cryogenic Layering

After sequential layering of MoF_6 and air, the spectrum (figure 2) initially displays the expected absorption bands associated with condensed phase water and CO_2: coupled intramolecular OH stretching modes around 3250 cm^{-1}, HOH bending modes at 1700 cm^{-1}, intermolecular librations at 900 cm^{-1}, the CO asymmetric stretching mode at 2350 cm^{-1}, and the OCO bending modes at 550 cm^{-1}. In addition, extra bands can be observed in the 700 cm^{-1} region which can be attributed to the cryogenically deposited MoF_6. The deposited MoF_6 exhibits three peaks red shifted, but spectrally similar, to gas phase MoF_6. Based on previous work[34-36], these peaks are identified as the ν_3 fundamental at 700 cm^{-1}, the $2\nu_4 + \nu_6$ combination band at 715 cm^{-1}, and the $3\nu_4$ overtone as a shoulder at 770 cm^{-1}.

Once the diamond substrate begins to warm, significant changes in the spectral features of all regions are observed. Initial changes in the MoF_6 spectral region are difficult to discern from simple phase changes due to the increase in temperature. Similar spectral changes were observed in the hydrolysis

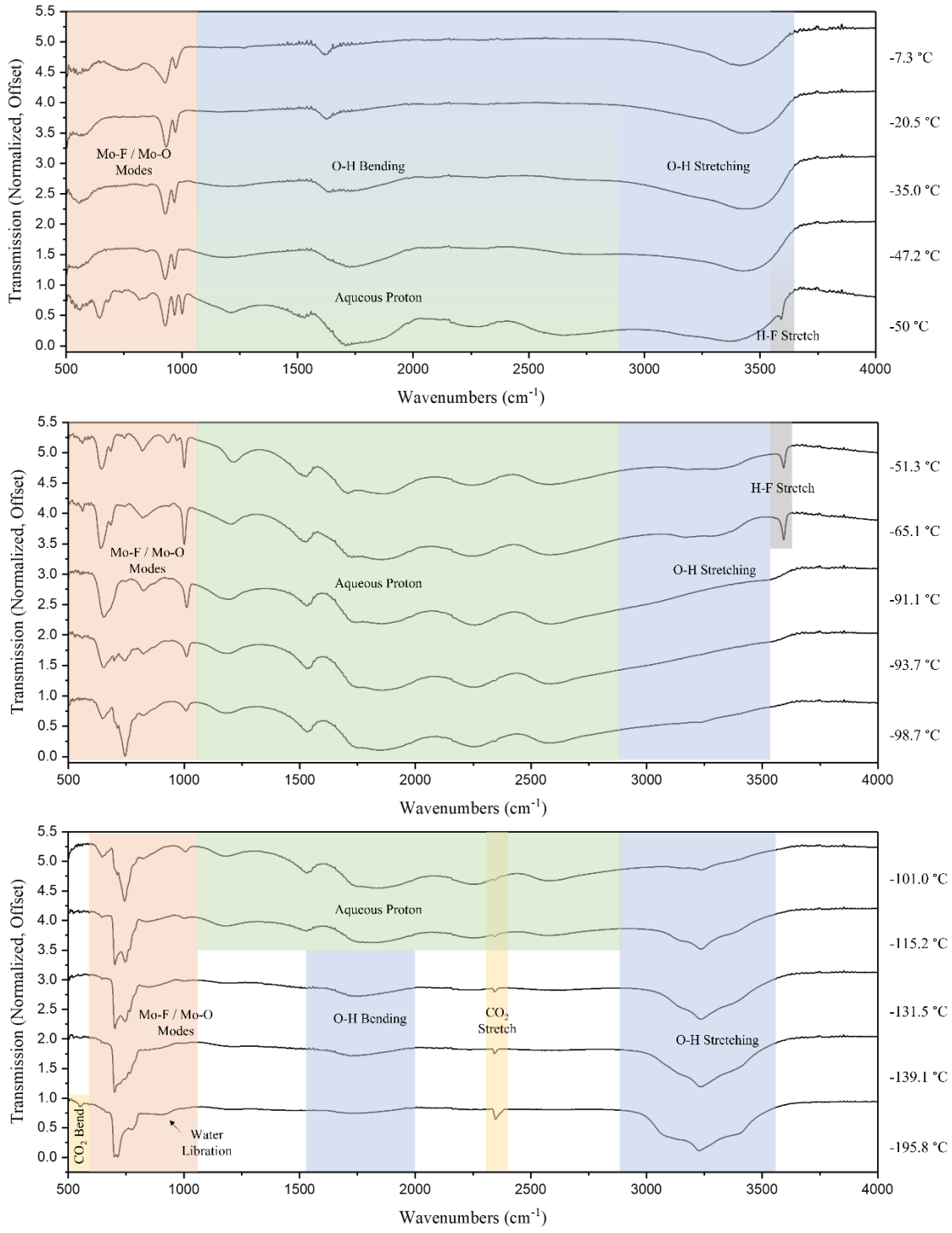

Figure 2 FTIR spectrum of the MoF_6 hydrolysis as temperature rises. Different regions have been color coded to correspond to known bands of water(blue), CO_2 (yellow), aqueous proton (green), and molybdenum fluorides/oxides (red). The experiment starts at -197.8 °C and warms up to -7.3 °C over the course of 2 hours.

reaction experiment and as changes observed upon allowing cryogenically deposited MoF_6 to warm up in the absence of water (Figure S1). There is also overlap between the spectral region associated with the intermolecular librations of water and the MoF_6 modes. These factors make it difficult to identify new species produced during the early steps of the hydrolysis reaction, i.e. at temperatures below -100 °C. However, as the reaction proceeds, a clear deviation from the pure MoF_6 warming spectra are observed and reaction intermediates can be identified. As expected, the signature peaks of CO_2 disappear as the substrate warms up - the CO_2 sublimates and is pulled off by the vacuum. The CO_2 sublimation happens concurrently with the depletion of the water OH stretching modes past 3000 cm^{-1} and the in-growth of a broad continuous absorption band from

roughly 1000-3000 cm^{-1}. The broad continuum of peaks in this intermediate region persists through the reaction until the final product is formed.

The continuum observed during the progression of the reaction is the spectroscopic signature of aqueous protons and is spectrally similar to previously reported spectra of HF dissociated in amorphous solid water[37]. Very broad and intense absorbance features initially appear around 1200 cm^{-1}, 1500 cm^{-1}, 1850 cm^{-1}, 2250 cm^{-1}, and 2550 cm^{-1}. After more time, two new features grow in around 3300 cm^{-1} and 3600 cm^{-1}. The large continuum provides evidence that fluorine atoms have been hydrolyzed from MoF_6 and are dissolved in an extended hydrogen bonded network. The spectral features of the aqueous proton-type continuum have been heavily studied, though there is still a healthy debate in the literature over the origin of many of these features. The unique method by which the network was created, and reaction monitored, allows for the results to provide some clarity on the debate.

The 1200 cm^{-1} band lies in an ambiguous spectral range based on previous experimental and computational studies[38-47]. Experimental data and electronic structure calculations suggest the intramolecular acidic proton symmetric stretching and bending modes of proton shared species, as well as several asymmetric vibrational modes of proton shared species and the symmetric bending umbrella mode of the Eigen-type cations are all expected to contribute oscillator strength around 1200 cm^{-1}. In the observed hydrolysis reaction of MoF_6, spectral shifting of the bands position and peak shape are associated with the presence of HF stretching in the extended network. The band blue shifts from 1175 cm^{-1} to 1215 cm^{-1} in the presence of HF and becomes noticeably more defined. The band then red shifts back to 1175 cm^{-1} as the HF is pulled off by vacuum. The changes in the band location suggests a proposed proton shared species such as $[H_2O{\bullet}HF](aq)$ are primarily responsible for contributing to the oscillator strength around 1215 cm^{-1} when an increased concentration of HF appears to be present. Species not directly sharing a proton with HF are then the major contributors around 1175 cm^{-1}.

The large band centred near 1850 cm^{-1} overlaps with the OH bending mode around 1700 cm^{-1} and has historically been assigned to Eigen-type ions asymmetric bending vibrations[39, 41-43, 45, 48]. However, there is literature which also supports the role of acidic proton asymmetric stretching vibrations of proton-shared species as more compelling candidates[37, 47, 49, 50]. Here, the 1850 cm^{-1} band appears well before the water OH stretching region completely depletes and remains constant through the change in HF concentration, even persisting after the HF has been removed from the reaction. The intensity of this band appears to be independent of HF concentration in the performed experiment and only depends on the presence of fluoride ions, which supports the Giguere and Turrell $[F^{-}{\bullet}H_3O^{+}](aq)$ contact ion pair model[51].

The broad band at 2550 cm^{-1} is attributed to either product-like Eigen-type $H_3O^{+}(aq)$ ions, which display a similar spectral feature as observed in amorphous mixtures of the strong acids HCl and HBr[52, 53], or OH stretching vibrations from strongly distorted water molecules in the first shell of fluoride anions[54-56]. The band has also been attributed to HF molecules bound to tetra-coordinated water[57]. Again, here the band is independent of HF concentration, leading to the conclusion that molecular HF is not directly involved in species contributing to oscillator strength in this area.

The region between 500 cm^{-1} and 1000 cm^{-1} is of much greater interest to the authors as it contains the relevant Mo-F and Mo-O stretching modes. Unfortunately, most spectroscopic data for MoF_6 has been collected in the gas phase, and there is limited research on MoF_6 hydrolysis, significantly complicating the identification of unique species in this range. The initial peaks around 700-780 cm^{-1} can be attributed to pure MoF_6 and identification of the product reveals the peaks in 500-1000 cm^{-1} region to be associated with MoO_3 hydrates, providing an overall reaction scheme of $MoF_6 + 3H_2O \rightarrow MoO_3 + 6HF$. Since the initial steps of the reaction are convoluted by changes in phase, working in reverse simplifies band determinations.

The product shows four distinct bands between 500-1000 cm^{-1} and two bands associated with water bending and stretching at 1700 cm^{-1} and 3400 cm^{-1}, respectively. The two bands between 900-1000 cm^{-1} can be identified as Mo=O stretching based on the product identification and previous experimental data[25-32]. These two bands appear early in the reaction and can be seen after the presence of HF is detected. As the reaction proceeds, these two peaks grow in stronger and remain the only peaks in the spectral region after HF has been fully removed. The band around 550 cm^{-1}, attributed to O-Mo-O bending[25-32], appears much earlier in the reaction and is correlated with the disappearance of HF in the spectra. These three peaks seen in the penultimate stage of the reaction are attributed to the formation of the molecular product MoO_3 during the final stages of the reaction. At this point in the reaction, the aqueous proton network is depleting due to the evaporation of H_2O and HF, and the MoF_6 has been fully hydrolyzed to MoO_3. The remaining peak at 750 cm^{-1} grows in much later than the other bands and is typically observed in large aggregates or nanoparticles of MoO_3 and water. The presence and timing of the 750 cm^{-1} suggest the band is due to the aggregation of the molecular MoO_3 hydrate and the formation of particulates in the condensed phase[58-63].

Moving back a step in the reaction process from the end-product, three distinct bands are present across the intermediate reaction (from approx. -50°C to -100°C), 650 cm^{-1}, 850 cm^{-1}, 1000 cm^{-1}, which all disappear along with the depletion of HF and appear with the formation of the extended aqueous proton network. Based on literature[25, 64-68], the peak at 1000 cm^{-1} is consistent with Mo=O stretching in neutral molybdenum fluorido-oxido compounds as well as molybdenum oxide stetching in similar anionic systems. Since our reaction is taking place surrounded by water the intermediates formed will be stabilized by the extended hydrogen bonding network of the aqueous proton. The molybdenum oxygen modes in both neutral and anionic systems are represented here as $[MoO/MoO^{-}][H_{net}]$. Since the 650 cm^{-1} and 850 cm^{-1} bands are heavily correlated to the mode at 1000 cm^{-1}, these major bands may be attributed to Mo-F stretching, bridged Mo-O-Mo, and bridged Mo-F-Mo modes.

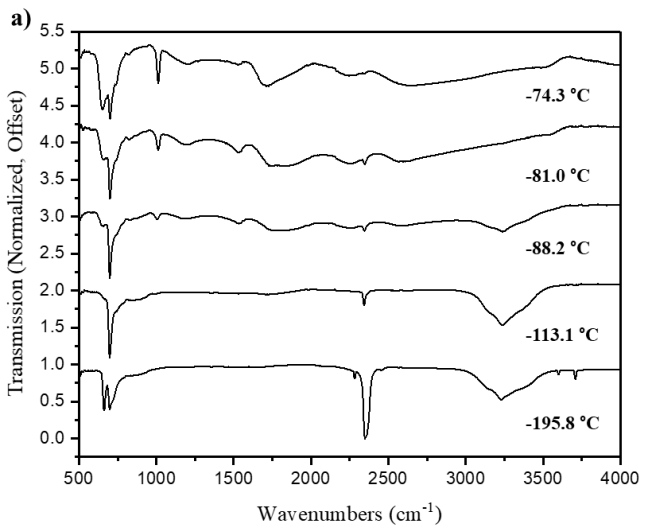

Figure 3 FTIR spectrum of the MoF_6 hydrolysis once an insulating layer of CO2 has been used depletion of the insulating CO_2 later and formation of aqueous proton network and b) Reactio increasing from bottom to top.

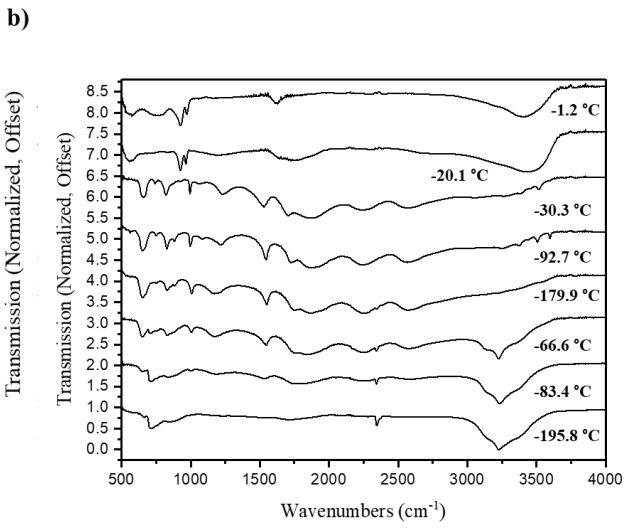

Figure 4 FTIR spectrum of the MoF_6 hydrolysis while refreezing the sample. Liquid nitrogen was added to the cryocell to refreeze the sample in between each spectrum. During this process, the sample was allowed to cool down to -195.8°C and warm back up to the labelled temperatures where the reaction proceeded.

Bridged Mo-F-Mo formation is common in these types of copounds; however, the reaction is taking place in a water network, so bridged Mo-O-Mo intermediates are also considered here and may be difficult to spectroscopically differentiate from Mo-F-Mo bridging. There are several other minor peaks and shoulders between 650-850 cm^{-1}, which are difficult to characterize due to low intensity and limited literature on the reaction, but are likely associated with intermediate and bridged compounds. Assuming a similar reaction pathway as proposed for UF_6 hydrolysis, the initial intermediate from the MoF_6 hydrolysis will likely be MoF_5OH, which should then quickly react to form $MoOF_4$. Knowing the final product to be fully hydrolyzed, fluorine atoms must be continually hydrolyzed, and a range of possible intermediates can be generated consisting of various hydroxylated molybdenum oxide fluorides. The list of possible intermediates makes it difficult to assign specific bonds to the bands observed between 500-1000 cm^{-1} during the intermediate steps of the hydrolysis reaction. In Particular, the peak at 850 cm^{-1} is difficult to assign and does not align with reported Mo-F or Mo=O stetching. Bridged Mo-O stetching has been attributed to this region for molybdenum oxides[28], but the band appears to grow in before the formation of molybdenum oxides in our experiment. Future computational studies may contribute significantly to the elucidation of possible intermediate species during the reaction.

Previous literature[65, 66] has reported Mo=O stretching frequencies for $MoOF_4$ to be between 1030-1048cm^{-1} and MoO_2F_2 Mo=O frequencies to be around 1009cm^{-1}. These numbers align well with the 1000cm^{-1} band observed in the reaction, but the Mo-F stretching frequencies of these compounds are typically observed in the 700-750cm^{-1} range. The Mo-F stretching bands in this experiments appear at at 650cm^{-1}, which is closer to the frequencies observed in MoF_5O^- and fluorine bridged $Mo_2F_9O_2^-$ comounds. The feature observed around 750cm^{-1} is in line with previously reported hydroxylated moldbdenum oxides and also with fluorine bridged compounds[25, 64-68].

The spectra initially show the reactant species modes, then MoF_6 and H_2O associated modes begin to disappear, and bands attributed to $[MoO/MoO^-][H_{net}]$ are generated. Next, the bands attributed to $[MoO/MoO^-][H_{net}]$ disappear as bands associated with MoO_3 appear. Finally, a band attributed to the formation of MoO_3 hydrate particulates grows in. The progression of the bands within the 500-1000 cm^{-1} region and the depletion and subsequent regeneration of defined OH stretching bands leads to the proposed reaction pathway presented in Scheme 1.

Scheme 1. Proposed reaction for condensed phase MoF_6 hydrolysis.

Step 1	$MoF_6(s) + 2H_2O(s) \rightarrow MoF_5O^-(s) + H_3O^+(s) + HF$
Step 2	$MoF_5O^-(s) + H3O^+(s) \rightarrow MoF_4O(s) + HF(s) + H_2O(s)$
Step 3	$MoF_4O(s) + 2H_2O(s) \rightarrow MoF_3O_2^-(s) + H_3O^+(s) + HF$
Step 4	$MoF_3O^-(s) + H_3O^+(s) \rightarrow MoF_2O_2 + HF(s) + H_2O(s)$
Step 5	$MoF_2O_2(s) + 2H_2O(s) \rightarrow MoFO_3^-(s) + H_3O^+(s) + HF$
Step 6	$MoFO_3^-(s) + H_3O^+(s) \rightarrow MoO_3(s) + HF(s) + H_2O(s)$
Step 7	$MoO_3(s) + 3H_2O(s) \rightarrow MoO_3 \bullet 3H_2O(s)$
Overall	$MoF_6(s) + 6H_2O(s) \rightarrow MoO_3 \bullet 3H_2O(s) + 6HF(s)$

The proposed reaction steps explain the appearance of the broad continuous aqueous proton bands which appear and is in line with previously reported hydrolysis products of MoF_6. Since the experiment was performed under vacuum, HF and excess water were likely pulled off and are not present in the final product.

Addition of CO_2 Insulating Layer

The experiment was also conducted using a CO_2 insulating layer between MoF_6 and H_2O, Figure 3. The insulating layer was added to ensure the reaction between the MoF_6 and water could not proceed at liquid nitrogen temperatures. Although this experiment confirms that an insulating layer is not necessary to prevent the hydrolysis reaction under the non-insulated experimental conditions, the subsequent reaction pathway has several noticeable differences from the initial experiment. The differences in the two experiments could be attributed to the increased temperature of the reactants upon initial contact. In the non-insulated experiment, the Boltzmann distribution of the thermal energy of the reactants results in many of the steps of the reaction overlapping. In the experiment with the insulating layer, all the reactants have been brought up to the temperature required to boil off CO_2 (approx. -140 ºC under vacuum conditions) before interaction begins. As a result, most of the reactants in the experiment with the insulating layer have enough energy for the reaction to proceed as soon as the insulating layer has been removed. The reaction proceeds in a much clearer, stepwise fashion which considerably reduces the number of overlapping bands in the 500 – 1000 cm^{-1} region.

The HF stretching mode around 3600 cm^{-1} behaves much more consistently with the proposed reaction pathway. The 3600 cm^{-1} band is initially absent and grows in, starting weak and broad before increasing in intensity and becoming sharper over time. The HF is likely being pulled off by the vacuum dissolved in the amorphous solid water network[37]. As the reaction progresses, the HF concentration reaches a point where the HF stretching mode can be detected. The excess water and HF is eventually boiled off and water is regenerated in the final step of the reaction forming a MoO_3 hydrate complex.

The band around 850 cm^{-1} that appears concurrently with the assigned $[Mo{=}O/MoO^{-}][H_{net}]$ stretching mode in the non-insulated experiment is significantly suppressed in the insulating layer experiment, as well as many of the minor peaks within the 500-1000 cm^{-1} range. Assignment of the bands during the intermediate portion of the reaction between 500-1000 cm^{-1} was difficult in the original experiment due to the large number of possible intermediate species. These bands were attributed primarily to the formation of bridged compounds. The absence of these bands in the insulating layer experiment suggests they are not the result of simple sequential hydrolysis, but rather due to some intermediate or dimer complex formation which is either not forming or has a lifetime too fast to resolve under the reaction conditions created by adding an insulating layer of CO_2.

Refreezing Experiment

Refreezing of the reaction was done by addition of liquid nitrogen to the Dewar and re-cooling the cold finger after the reaction had begun, Figure 4. Re-cooling the cold finger "froze" the reactions in place, preventing the reaction from proceeding and sharpening many of the bands associated with the intermediate steps. The refreezing of the reaction had no

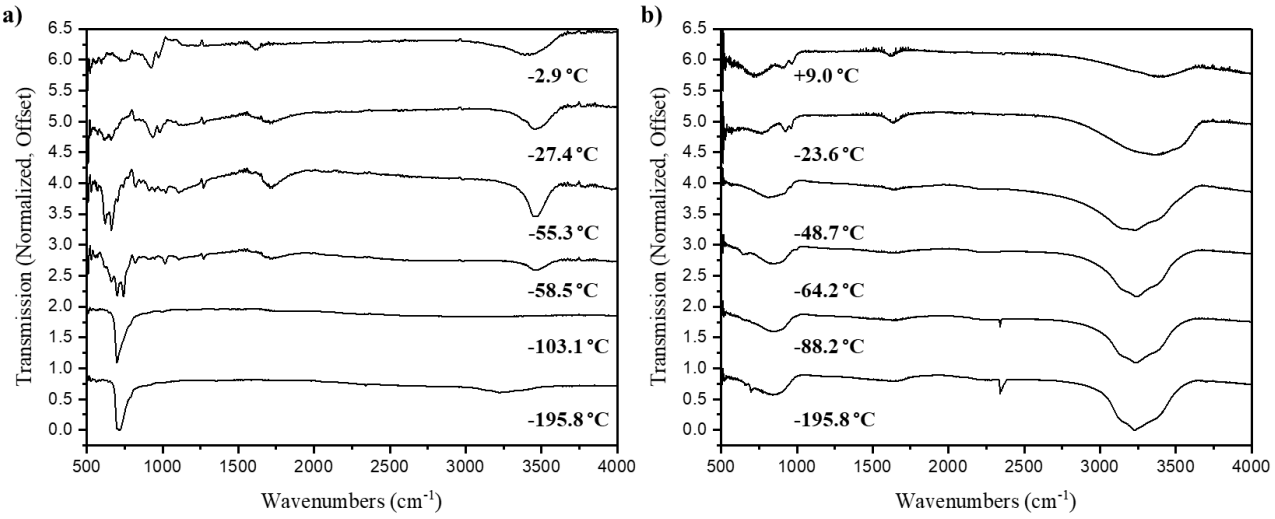

Figure 5 FTIR spectrum of the MoF_6 hydrolysis under different limiting reactant conditions. a) limiting the amount of water layered on top of a thick layer of MoF6 layer, and b) limiting the amount of MoF_6 initially layered followed by a thick layer of air to ensure excess water is present for the reaction. For each condition, reactants were allowed to slowly warm to room temperature while the IR spectrum was monitored.

conditions of the experiment before the defined OH stretching water bands begin to grow in. Since HF is a by-product of the initial reaction step the appearance of an HF band is expected quite early in the reaction. HF ingrowth is predicted to run concurrently with the initial depletion of the water bands. The hydrolyzing of the fluorine is observed by the development of the aqueous proton network, which is the result of HF being impact on the formation of the final product. The intermediate bands between 500 cm^{-1} and 1000 cm^{-1} can be captured with the minor peak and shoulder between 650 cm^{-1} and 850 cm^{-1} appearing as they did in the original experiment. Both the minor peak and shoulder grow in around the same time, but the shoulder peak around 850 cm^{-1} is completely depleted before the minor peak around 650 cm^{-1} disappears. In addition,

multiple sharp peaks appear in the HF stretching region, suggesting the HF produced is not trapped in a uniform network.

Effect of Reactant Concentrations

The relative ratio of MoF_6 and water were varied to assess the impact of limiting reactants on the overall reaction path and product production, Figure 5. Limiting the amount of water did not affect the formation of the final product and the general progression of the reaction is also unaltered. Therefore, the conclusion was drawn that the extended hydrogen bonding and aqueous proton networks are not required for the reaction to proceed to completion, which should be true since gas phase hydrolysis of MoF_6 is possible. Interestingly, the final product is spectrally different when MoF_6 is the limiting reactant. In the MoF_6-limited case, the 750 cm^{-1} band attributed to the aggregation of MoO_3 hydrates appears earlier and is much broader in the final product while the 650 cm^{-1} band does not appear or is obscured. The change in these two bands must be attributed to the large excess of water still around during the formation of the MoO_3. In the previous experiments, all the well-defined OH stretching has disappeared before the transition from molecular MoO_3 hydrate to MoO_3 hydrate particulates. This suggests that excess water was not being pulled off by vacuum, but instead water was acting as the limiting reactant of the hydrolysis and was being completely consumed. When MoF_6 is the limiting reactant, the excess water appears to have facilitated particulate aggregation.

Conclusions

The work described herein reports a detailed spectroscopic study of the hydrolysis reaction of MoF_6. The reaction intermediates were demonstrated to be trapped in the disordered H-bonded network of a cryogenic amorphous thin film formed by sequential deposition of MoF_6 and H_2O followed by heating. The hydrolysis reaction does not require the presence of the H-bonded network to proceed, but the relative abundance of H_2O does affect the condensed phase particulate formation. An insulating layer can be used to separate the two reactants but is not necessary to prevent the spontaneous hydrolysis of MoF_6 at liquid nitrogen temperatures. A simple reaction pathway was proposed for the hydrolysis of MoF_6 based on the available spectroscopic data and product identification.

Even though the final product of this reaction is not identical to the corresponding UF_6 hydrolysis reaction, understanding the hydrolysis process for MoF_6 can lead to more informed predictions for UF_6 hydrolysis. The work also demonstrated the ability for the condensed phase hydrolysis of MoF_6 to result in particulate formation and for the particulates to be a function of the available water. Assuming similar pathways of particulate formation for UF_6, it would be expected that condensed phase particulates can also form.

Experimental

Cryogenic Layering

A cryogenic cell was custom designed at Savannah River National Laboratory to perform experiments at liquid nitrogen temperatures. The cell was held at vacuum and was made with 2-inch diameter uncoated zinc selenide windows from Edmund Optics in order to view the samples, which were deposited onto a 18 mm diameter, 150 µm think polished polycrystalline diamond window from Applied Diamond, Inc.. A diamond surface was chosen as a substrate due to its transparency in the infrared and excellent thermal conductivity. The substrate was mounted on a copper cold finger extended from an open liquid nitrogen Dewar. The temperature of the cold finger was controlled by liquid nitrogen in the Dewar as the cold finger could be kept at liquid nitrogen temperatures by the addition of liquid nitrogen to the Dewar or warmed by allowing the liquid nitrogen to evaporate and exposing the copper cold finger to room temperature. The cryogenic cell was attached to a volume calibrated gas manifold which was used to control the amount of gas condensed onto the surface of the substrate. Thin films could be deposited onto the clean diamond surface after it has been cooled to -198 °C by backfilling the chamber with gaseous samples admitted through a high-precision leak valve. Gaseous samples of MoF_6 were admitted from high purity cylinders, purchased from Alfa Aesar, through the gas manifold, while atmospheric water and carbon dioxide were admitted via a controlled air leak onto the substrate. The layers were generated separately to calibrate the gas flow from the manifold to the cryogenic cell and control the thickness of the individual layers (S2). Once the samples were layered on the diamond surface, reactions were monitored in a Jasco FT-IR 6300 (Jasco Inc, Easton, MD, USA) while the layers were allowed to heat to room temperature over the course of 4 to 5 hours. A scan was taken every 30 seconds with a 2 cm^{-1} resolution and a 400 to 6000 cm^{-1} spectral range. The cold finger temperature was monitored using a thermocouple mounted to the end of the copper rod and digitally recorded over the course of the reaction using a DAC and LabVIEW program.

UV/Vis

The product was collected from the diamond substrate via a cotton swap and dissolved in D.I. water. The resulting liquid was then analysed with a custom-built UV – Vis using a xenon lamp light source.

Scanning Electron Microscopy

In order to collect product to be analysed with scanning electron microscopy (SEM), small carbon wafers were placed at the bottom of the cryogenic cell and a standard reaction was set up and executed. The wafers were then collected and analysed with a JEOL 2010 TEM and Hitachi SU8200 SEM.

Conflicts of interest

There are no conflicts to declare.

Acknowledgements

This work was produced by Battelle Savannah River Alliance, LLC under Contract No. 89303321CEM000080 with the U.S. Department of Energy. Publisher acknowledges the U.S. Government license to provide public access under the DOE Public Access Plan (http://energy.gov/downloads/doe-public-access-plan). Financial support for this work was provided by the National Nuclear Security Administration under Defense Nuclear Nonproliferation R&D. Assistance from Dr. Daniel Morrall at SRNL with TEM and SEM/EDS is gratefully acknowledged.

Notes and references

1. J. Bigeleisen, M. G. Mayer, P. C. Stevenson and J. Turkevich, *The Journal of Chemical Physics*, 1948, **16**, 442-445.
2. B. Weinstock and R. H. Crist, *The Journal of Chemical Physics*, 1948, **16**, 436-441.
3. R. DeWitt, *Uranium Hexafluoride: A Survey Of The Physicochemical Properties*, United States, 1960.
4. G. P. Verkhivker, S. D. Tetel'baum and G. P. Konyaeva, *Soviet Atomic Energy*, 1968, **24**, 191-195.
5. J. Fuger, *The Actinide Halides*, International Atomic Energy Agency, 1983.
6. I. "Grenthe, J. "Fuger, R. J. "Lemire, A. B. "Muller, C. "Nguyen-Trung Cregu and H. "Wanner, *Chemical thermodynamics of uranium*, Amsterdam (Netherlands); Elsevier Science Publishers;, Netherlands, 1992.
7. *Uranium hexafluoride: A manual of good handling practices. Revision 7*, United States, 1995.
8. M. J. Z. a. S. G. B. J. McBride, *Journal*, 2002.
9. P. W. Pickrell, *Characterization of the solid, airborne materials created when UF/sub 6/ reacts with moist air flowing in single-pass mode*, United States, 1985.
10. W. D. Bostick, W. H. McCulla and P. W. Pickrell, *Sampling, characterization, and remote sensing of aerosols formed in the atmospheric hydrolysis of uranium hexafluoride*, United States, 1984.
11. R. W. Kessie, *Industrial & Engineering Chemistry Process Design and Development*, 1967, **6**, 105-111.
12. D. P. Armstrong, W. D. Bostick and W. H. Fletcher, *Applied Spectroscopy*, 1991, **45**, 1008-1016.
13. S. A. Sherrow and R. D. Hunt, *The Journal of Physical Chemistry*, 1992, **96**, 1095-1099.
14. R. Kips, A. Leenaers, G. Tamborini, M. Betti, S. Van den Berghe, R. Wellum and P. Taylor, *Microscopy and Microanalysis*, 2007, **13**, 156-164.
15. R. S. Kips and M. J. Kristo, *Journal of Radioanalytical and Nuclear Chemistry*, 2009, **282**, 1031.
16. R. Kips, M. J. Kristo, J. C. Crowhurst and I. D. Hutcheon, 2010.
17. G. L. Wagner, S. A. Kinkead, M. T. Paffett, K. D. Rector, B. L. Scott, A. L. Tamasi and M. P. Wilkerson, *Journal of Fluorine Chemistry*, 2015, **178**, 107-114.
18. S. R. Hanna, J. C. Chang and X. J. Zhang, *Atmospheric Environment*, 1997, **31**, 901-908.
19. S. L. Garrison and J. M. Becnel, *The Journal of Physical Chemistry A*, 2008, **112**, 5453-5457.
20. S.-W. Hu, X.-Y. Wang, T.-W. Chu and X.-Q. Liu, *The Journal of Physical Chemistry A*, 2008, **112**, 8877-8883.
21. S.-W. Hu, X.-Y. Wang, T.-W. Chu and X.-Q. Liu, *The Journal of Physical Chemistry A*, 2009, **113**, 9243-9248.
22. M. C. Lind, S. L. Garrison and J. M. Becnel, *The Journal of Physical Chemistry A*, 2010, **114**, 4641-4646.
23. S.-W. Hu, H. Lin, X.-Y. Wang and T.-W. Chu, *Journal of Molecular Structure*, 2014, **1062**, 29-34.
24. J. J. Lutz, J. N. Byrd, V. F. Lotrich, D. S. Jensen, J. Zádor and J. A. Hubbard, *Physical Chemistry Chemical Physics*, 2022, **24**, 9634-9647.
25. B. F. Hoskins, A. Linden and T. A. O'Donnell, *Inorganic Chemistry*, 1987, **26**, 2223-2228.
26. L. Seguin, M. Figlarz, R. Cavagnat and J. C. Lassègues, *Spectrochimica Acta Part A: Molecular and Biomolecular Spectroscopy*, 1995, **51**, 1323-1344.
27. G. Guzman, B. Yebka, J. Livage and C. Julien, *Solid State Ionics*, 1996, **86-88**, 407-413.
28. M. Dieterle and G. Mestl, *Physical Chemistry Chemical Physics*, 2002, **4**, 822-826.
29. A. Chithambararaj and A. C. Bose, *Beilstein J Nanotechnol*, 2011, **2**, 585-592.
30. A. Klinbumrung, T. Thongtem and S. Thongtem, *Journal of Nanomaterials*, 2012, **2012**, 930763.
31. C. Angamuthuraj, S. n s, A. Bose and S. Velmathi, *Catalysis Science & Technology*, 2013, **3**, 1405.
32. N. Maheswari and G. Muralidharan, *Applied Surface Science*, 2017, **416**, 461-469.
33. C. Julien and G. A. Nazri, *Solid State Ionics*, 1994, **68**, 111-116.
34. T. G. Burke, D. F. Smith and A. H. Nielsen, *The Journal of Chemical Physics*, 1952, **20**, 447-454.
35. H. H. Claassen, H. Selig and J. G. Malm, *The Journal of Chemical Physics*, 1962, **36**, 2888-2890.
36. R. S. McDowell, R. J. Sherman, L. B. Asprey and R. C. Kennedy, *The Journal of Chemical Physics*, 1975, **62**, 3974-3978.
37. P. Ayotte, S. Plessis and P. Marchand, *Physical Chemistry Chemical Physics*, 2008, **10**, 4785-4792.
38. L. H. Jones and R. A. Penneman, *The Journal of Chemical Physics*, 1954, **22**, 781-782.
39. C. Lee, C. Sosa, M. Planas and J. J. Novoa, *The Journal of Chemical Physics*, 1996, **104**, 7081-7085.
40. T. v. Rosenvinge, M. Parrinello and M. L. Klein, *The Journal of Chemical Physics*, 1997, **107**, 8012-8019.
41. S. Re, *The Journal of Physical Chemistry A*, 2001, **105**, 9725-9735.
42. E. M. Cabaleiro-Lago, J. M. Hermida-Ramón and J. Rodríguez-Otero, *The Journal of Chemical Physics*, 2002, **117**, 3160-3168.
43. S. Odde, B. J. Mhin, S. Lee, H. M. Lee and K. S. Kim, *The Journal of Chemical Physics*, 2004, **120**, 9524-9535.
44. J. P. Devlin, M. W. Severson, F. Mohamed, J. Sadlej, V. Buch and M. Parrinello, *Chemical Physics Letters*, 2005, **408**, 439-444.
45. S. Odde, B. J. Mhin, K. H. Lee, H. M. Lee, P. Tarakeshwar and K. S. Kim, *The Journal of Physical Chemistry A*, 2006, **110**, 7918-7924.
46. E. S. Stoyanov and C. A. Reed, *The Journal of Physical Chemistry A*, 2006, **110**, 12992-13002.
47. R. Iftimie, V. Thomas, S. Plessis, P. Marchand and P. Ayotte, *Journal of the American Chemical Society*, 2008, **130**, 5901-5907.

48. P. A. Giguère, C. Martel and S. Turrell, *Chemical Physics Letters*, 1978, **56**, 231-234.
49. J. M. Headrick, E. G. Diken, R. S. Walters, N. I. Hammer, R. A. Christie, J. Cui, E. M. Myshakin, M. A. Duncan, M. A. Johnson and K. D. Jordan, *Science*, 2005, **308**, 1765-1769.
50. H. H. Hyman, M. Kilpatrick and J. J. Katz, *Journal of the American Chemical Society*, 1957, **79**, 3668-3671.
51. P. A. Giguere and S. Turrell, *Journal of the American Chemical Society*, 1980, **102**, 5473-5477.
52. L. Delzeit, B. Rowland and J. P. Devlin, *The Journal of Physical Chemistry*, 1993, **97**, 10312-10318.
53. J. P. Devlin, V. Buch, F. Mohamed and M. Parrinello, *Chemical Physics Letters*, 2006, **432**, 462-467.
54. K. Laasonen, *Molecular Physics*, 1996, **88**, 135-142.
55. K. Ando and J. T. Hynes, *The Journal of Physical Chemistry A*, 1999, **103**, 10398-10408.
56. A. J. Sillanpää, C. Simon, M. L. Klein and K. Laasonen, *The Journal of Physical Chemistry B*, 2002, **106**, 11315-11322.
57. J. M. Heuft and E. J. Meijer, *The Journal of Chemical Physics*, 2005, **122**, 094501.
58. A. Müller, J. Meyer, E. Krickemeyer and E. Diemann, *Angewandte Chemie International Edition in English*, 1996, **35**, 1206-1208.
59. A. Müller and S. Roy, *Coordination Chemistry Reviews*, 2003, **245**, 153-166.
60. T. Liu, E. Diemann, H. Li, A. W. M. Dress and A. Müller, *Nature*, 2003, **426**, 59-62.
61. S.-i. Noro, R. Tsunashima, Y. Kamiya, K. Uemura, H. Kita, L. Cronin, T. Akutagawa and T. Nakamura, *Angewandte Chemie International Edition*, 2009, **48**, 8703-8706.
62. E. Garrido Ribó, N. L. Bell, W. Xuan, J. Luo, D.-L. Long, T. Liu and L. Cronin, *Journal of the American Chemical Society*, 2020, **142**, 17508-17514.
63. B. Botar, A. Ellern and P. Kögerler, *Dalton Transactions*, 2012, **41**, 8951-8959.
64. W. K. Wal, *Journal of Molecular Structure*, 1984, **115**, 59-62.
65. B. G. Ward and F. E. Stafford, *Inorganic Chemistry*, 1968, **7**, 2569-2573.
66. I. R. Beattie, K. M. S. Livingston, D. J. Reynolds and G. A. Ozin, *Journal of the Chemical Society A: Inorganic, Physical, Theoretical*, 1970, DOI: 10.1039/J19700001210, 1210-1216.
67. R. Bougon, T. Bui Huy and P. Charpin, *Inorganic Chemistry*, 1975, **14**, 1822-1830.
68. R. E. Stene, B. Scheibe, A. J. Karttunen, W. Petry and F. Kraus, *European Journal of Inorganic Chemistry*, 2019, **2019**, 3672-3682.